

Mechanical and photosynthetic constraints on the evolution of plant shape

Karl J. Niklas and Vincent Kerchner

Abstract.—A computer model is presented which is capable of calculating both the photosynthetic efficiency (I) of any specified plant shape and the stress related to the total moment arm (M) imposed on vertical branching patterns. Computer simulations indicate that a flattened plant thallus and an erect branching growth habit are two plant shapes capable of optimizing photosynthetic efficiency during indeterminate growth. These two morphologies have geometric analogues in the dorsiventral thalli of some bryophytes and in the vertical axes of mosses and tracheophytes, respectively.

Extension of the model to complex, three-dimensional branching patterns indicates that I and I/M are maximized when branching is overtopped (treelike, with lateral branches on a main axis) and when lateral branching systems are planated (frondlike). Geometric alterations of branching patterns that result in optimization of I and I/M can be simulated by computer and are shown to be similar to morphologic alterations attending the early evolution of vascular land plants. It is suggested that a number of major evolutionary trends seen in Upper Silurian to Upper Devonian times can be expressed in terms of optimizing the display of photosynthetic tissues (I) or the balance between photosynthetic efficiency and incurred moment arms (I/M).

Karl J. Niklas and Vincent Kerchner. Section of Plant Biology, Cornell University, Ithaca, New York 14853

Accepted: September 10, 1983

Introduction

The selective pressures to gain greater access to light in competition with surrounding plants, and thus to gain height, would appear to be a very basic feature of the biology of plants. In conjunction with the benefits to photosynthetic processes, the production of vertical axes increases the potential dispersal range of spores or propagules borne on aerial branches. Thus, conventional paleobotanical thought has placed emphasis on photosynthetic and reproductive efficiency to account for the tendency of plants to evolve greater stature (Bower 1935; Zimmermann 1930; Banks 1968, 1972; Chaloner and Sheerin 1979; Niklas et al. 1980). The effect of vertical (orthotropic) growth on photosynthetic efficiency as it relates to plant evolution has never been addressed in a rigorous fashion. Nor has any attempt been made to integrate other features typical for aerial axis morphology (circular cross-section, branching, overtopping) within the context of selective pressures favoring increased stature. In particular, the relationship between the efficient display of photosynthetic surfaces and the consequent mechanical effects of the bending moments produced by unsupported axes must be of fundamental importance in defining plant shape (cf. Niklas and O'Rourke 1982).

This paper describes some of the inherent geometric and mechanical relationships relevant to the evolution of increased plant stature. The paleobiological context for this analysis is the initial radiation of the vascular land plant flora (Silurian/Devonian): (1) It was during the Early Paleozoic that plants responded to the various physiologic and mechanic constraints attending the transition from an aquatic to a terrestrial habitat. (2) As a consequence many of the features that distinguish the sporophytes of land plants were canalized (e.g., orthotropic aerial axes that are circular in cross-section and often branched), thereby defining subsequent evolutionary events (e.g., arborescence). (3) The range in plant shape, and presumably physiology, was sufficiently small to allow for necessary simplifying assumptions involved in modeling. And (4) knowledge of the fossil record of the early vascular land plants is sufficiently detailed to permit an evaluation of the predictions made by this study.

The Model

The efficiency of photosynthesis is a surface area to volume dependent factor, so it is axiomatic that morphology (geometry) influences photosynthesis at a fundamental level (Monsi

and Saeki 1953; Gates 1965, 1970; Nobel 1980, 1981, 1982). Photosynthetic efficiency, I , as used here, is not the same term as is used in plant physiology. The latter has the common connotation of "quantum efficiency," i.e., the efficiency of converting light energy into chemical energy. If it is assumed that light is a limiting factor, then the amount of light absorbed by any two morphologies can be directly assessed by means of a simple geometric relationship (namely, their respective projected surface area to total surface area ratio, or A_p/A). Provided that both morphologies are competing in the same light environment and with the same physiologic capacities to utilize radiant energy, the photosynthetic efficiency, I , for any organism can be computed as a function of the projected surface area to total surface area, multiplied by the irradiance (S_p) on surfaces perpendicular to the solar angle (Θ):

$$I = \int_{0^\circ}^{90^\circ} \frac{A_p}{A} S_p \cdot d\theta$$

For a clear day, S_p is relatively independent of the elevation angle and approximately equals 0.8–1 kw/m² (Anderson 1964). Thus S_p is a constant and the analysis between two or more plant shapes can be simplified to comparing their respective A_p/A values as a function of Θ .

$$I = \lim_{\Delta\theta \rightarrow 0^\circ} \sum_{\theta=0^\circ}^{\theta=90^\circ} \frac{A_p}{A}(\theta) \Delta\theta.$$

It might be argued that, for small plants, sunlight will penetrate through the entire width of the axis, thereby negating the relevancy of the A_p/A relationship in computing relative photosynthetic efficiency. This criticism is obviated by the fact that while light will penetrate, the importance of this penetration is limited by (1) the rate of attenuation and (2) the light compensation point for photosynthesis. The intensity of light passing through plant tissues diminishes in an apparently exponential manner with depth, in accordance with the equation

$$E_d(Z) = E_d(0)e^{-kz},$$

where $E_d(Z)$ is the inward irradiance (flux of energy per unit area per second) at depth Z , $E_d(0)$ is the level of irradiance just at the surface of the plant axis, and k is the vertical attenuation coefficient for light through the tissues. Based on

the values of k computed for a variety of plants, Z ranges in value from 1.0 to 3.5 mm—a range slightly in excess of the most probable maximum widths of early land plant axes. However, calculations indicate that for an axis 1.0 mm thick, the attenuation of light through the axis will result in an extremely reduced level (5%) of irradiance on the shaded portion (Monsi and Saeki 1953). This level of irradiance is roughly equivalent to the compensation point for photosynthesis. Thus, even though photosynthesis will occur in all photosynthetic tissues, the bulk of photosynthesis above the compensatory level will be on directly illuminated surfaces. This conclusion is indirectly supported by the geometry and distribution of chloroplasts in the leaves of living flowering plants and bryophytes. Further, if the photosynthetic tissues of the axis are assumed to be parenchymatous and protected by a cuticle without stomata, then the diffusion gradient of carbon dioxide (with an external concentration of the present day, 10 nmole·cm⁻³) is such that at a distance of 13.5 μm from the plant-air interface, the concentration of CO₂ equals 0.3 nmole·cm⁻³. The carboxylase activity at this CO₂ concentration in the axes of Silurian-Devonian plants would operate at less than 5% of the rate computed near the surface (epidermis). Thus, for plant axes greater than approximately 30 μm in diameter and without stomata, effective photosynthesis is limited to regions near the plant-air interface but is restricted due to irradiant energy attenuation to illuminated surfaces. In the presence of stomata, the effective volume of photosynthetic tissue is dramatically increased. However, it may be assumed that the presence of stomata on a fossil plant is associated with an axis of substantial thickness, with an intervening region of cortical and vascular tissues (the latter not involved in CO₂ fixation). Thus, for the purposes of comparing relative photosynthetic capacity, the A_p/A index fulfills the criteria of being a reasonable and biological measurement.

Similarly, it may seem more reasonable to compute relative photosynthetic performance on the basis of illuminated surface area (A_i) rather than on the basis of projected surface area (A_p). The irradiance at a surface depends on the orientation of the surface to light, since the radiant flux remains constant but the flux density varies. Photosynthetic rates are best assessed on the ba-

TABLE 1. Comparisons among the photosynthetic capacity ($I = \sum_{\theta=0^\circ}^{\theta=90^\circ} Ap/A(\theta)\Delta\theta$) of various plant morphologies in relationship to morphometric changes (d/l and l/d ; cf. Fig. 1) attending indeterminate growth. Numbers in parentheses give I as percentage of I_{max} for each geometry.

d/l	Spheroid		l/d	Cylinder (I)	Cylinder with hemispherical ends (I)
	Oblate (I)	Prolate (I)			
1.00	44.9 (57.1)	44.9 (100)	1	43.3 (100)	40.7 (100)
.50	50.1 (87.6)	35.7 (79.5)	2	40.6 (93.8)	39.2 (96.3)
.25	53.9 (94.2)	29.0 (64.6)	4	38.6 (88.7)	38.1 (93.6)
.10	54.8 (95.8)	24.3 (54.1)	10	37.4 (86.4)	37.2 (91.4)
.01	56.9 (99.5)	21.2 (47.2)	100	36.5 (84.3)	36.5 (89.7)
10^{-5}	57.2 (100)	20.8 (46.3)	10^5	36.3 (83.8)	36.3 (89.2)

sis of flux density; therefore, Ap/A provides a more realistic measure of photosynthetic efficiency.

The simplest shape that can be used to illustrate the Ap/A computation is a sphere, since its projected surface area is a circle; thus, the Ap/A ratio is given by

$$\frac{Ap}{A} = \frac{\pi r^2}{4\pi r^2} = \frac{1}{4}.$$

In this case, Ap/A is a constant and does not vary as a function of the solar angle, Θ . A spherical shape has the advantage of absorbing the maximum amount of irradiance per day in comparison to cones and cylinders and is suited in an environment where θ may vary randomly, as for example in the case of a spherical alga tumbling through the water column. On land, however, the sphere-shaped plant has two disadvantages: an increase in size progressively decreases its surface area to volume ratio as a function of the $2/3$ -power law and concomitantly decreases the surface area through which CO_2 and H_2O are absorbed (Niklas 1976).

Thus, with continued growth, a geometric alteration must attend an increase in size if photosynthesis and respiration requirements are maintained at a constant level. A geometric solution to this growth constraint is to progressively alter the spherical thallus into either an oblate or a prolate spheroid, that is, a solid formed by the rotation of an ellipse about its minor or major axis, respectively. The Ap/A ratio for an oblate spheroid, with a and b as its major and minor semiaxes, is

$$\frac{Ap}{A} = \frac{ap|\sin(\theta + \phi)|}{\pi 2a^2 + \pi b^2 \ln \frac{1+e}{1-e}},$$

where

$$p = \left(\frac{a^4 \tan^2 \theta + b^4}{a^2 \tan^2 \theta + b^2} \right)^{1/2}$$

and

$$\phi = \sin^{-1} \left(\frac{b^4}{a^2 \tan^2 \theta + b^2} \right)^{1/2}.$$

The relationship between Ap/A and $0^\circ \leq \Theta \leq 90^\circ$ is shown in Fig. 1A. With a progressive increase in size, the "depth to length" ratio, d/l , of the thallus must progressively decrease if the surface area to volume ratio, S/V , is to be maintained. As d/l decreases, the area under the

Ap/A versus Θ curve (i.e., $\sum_{\theta=0^\circ}^{\theta=90^\circ} \frac{Ap}{A}(\theta)\Delta\theta$)

increases, indicating that "flattening" of an oblate spheroid enhances its photosynthetic capacity (Table 1). This geometric solution to increased absolute size with a constant S/V has a biologic analogue in the thalloid liverworts, which produce a dorsiventral plant body. The increase in photosynthetic capacity (Table 1), however, presumes that sunlight reaches the thallus from $0^\circ \leq \Theta \leq 90^\circ$, i.e., that the plant is growing in an unobstructed, totally flattened topography. Irregularities in the topography would severely reduce the photosynthetic efficiency, e.g., for an oblate spheroid with $d/l = 0.5$, growing in an environment in which Θ was restricted to $20^\circ \leq \Theta \leq 80^\circ$, the photosynthetic efficiency would be reduced by 43%.

Similarly, the Ap/A ratio for a prolate spheroid is given by

$$\frac{Ap}{A} = \frac{1 + (x - 1)\cos \theta}{2x + \frac{2 \sin^{-1}(1 - x^2)^{1/2}}{(1 - x^2)^{1/2}}},$$

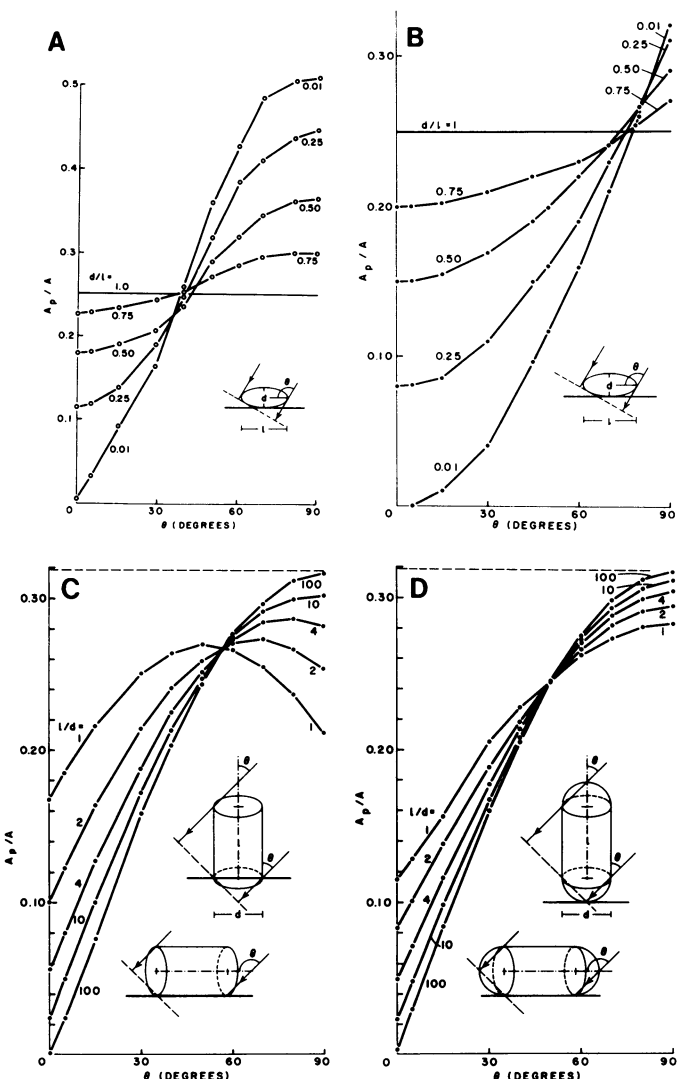


FIGURE 1. The relationship between the projected area to total surface area ratio (A_p/A) and the solar angle (Θ) for an oblate (A) and prolate (B), and for a cylinder (C) and cylinder with hemispherical ends (D). The solar angle, Θ , is defined as the angle between the major axis (l) of the spheroid or the length (l) of the cylinder and solar irradiance (arrows in inserts). The projected area (A_p) is on a surface normal to solar irradiance (dashed lines in inserts). A, For an oblate spheroid (an ellipse rotated about its minor axis, d), as d/l decreases, I increases. B, For a prolate spheroid (an ellipse rotated about its major axis, l) as d/l decreases, I increases. C, D, For cylindrical geometries, as l/d increases, I decreases but exceeds the minimum I value of a prolate spheroid (cf. Table 1).

where x is the depth to length ratio (cf. Fig. 1B). With a progressive increase in absolute size the depth to length ratio of the thallus must progressively decrease if the physiologically requisite surface area to volume ratio, S/V , is to be maintained. The consequences of this alteration in geometry on light absorption are pronounced and illustrated graphically in Fig. 1B. As the

d/l ratio declines, the “area” under the A_p/A versus Θ graph declines sharply (Fig. 1B). The area under the A_p/A versus Θ graph is a direct representation of the amount of radiant energy absorbed (on a diurnal basis) by the plant body. The decline in area is due to the simple fact that at low Θ -values (at and shortly after dawn), the thallus “projects” very little of its surface area.

Of interest, also, is the fact that the orientation of the thallus that maximizes the Ap/A value is around noon, where heat gain and water loss are presumably at their near maximum values (Gibbs and Patten 1970; Konis 1950; Nisbet and Patten 1974; Woodhouse et al. 1980).

Another geometric solution to indeterminate growth and the maintenance of a requisite surface area to volume ratio is the distortion of a sphere or prolate spheroid into a cylinder. For such a geometry,

$$\frac{Ap}{A} = \frac{b|\sin \theta| + \frac{d}{4}|\cos \theta|}{\frac{d}{4} + b}.$$

The elongation of a cylindrical thallus will accommodate growth and maintain a constant surface area to volume ratio, even though the length to depth ratio (l/d) of the entire plant increases (Fig. 1C). It can be seen that the consequences of this mode of geometric distortion on the Ap/A curve are similar to those for the previous prolate spheroid, since the value of the area under the Ap/A curve steadily declines. However, the minimum limit to the area under the Ap/A curve (I) is 0.318, in contrast to that of the prolate spheroid, which is 0.182 (Table 1). Thus the Ap/A area limit of the cylindrical plant body is 57.2% greater than that of a prolate spheroid. If the spheroid and cylindrical modes of geometric solutions to S/V and Ap/A are compared, it is mathematically self-evident that the prolate spheroid solution is less photosynthetically competitive than the extending cylinder solution. This conclusion is unaltered even if a hemispherical shape surmounts either end of the cylinder so as to "mimic" an apical meristem or an attenuated tip (Fig. 1D; Table 1).

In the extreme case, a cylindrical thallus can be oriented either flush with the substrate or in a vertical manner. Analyses indicate that the vertical orientation is preferred for photosynthesis, since (1) it maximizes the projected area of the cylinder to the solar angle, in contradistinction to a prostrate cylinder that may be shaded by topography of the microhabitat, and (2) it minimizes its surface area at noon ($\Theta = 90^\circ$). Thus, orthotropic growth of a cylindrical axis can be

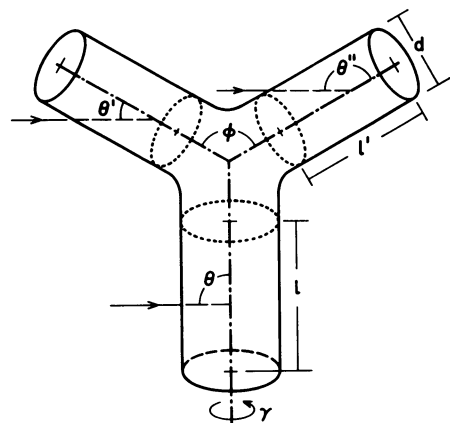


FIGURE 2. Branched telome or single bifurcation resulting from the joining (dotted circles) of three cylindrical elements. For purposes of simplicity, each cylindrical element has the same length ($l = l'$) and diameter (d). Dependent upon the bifurcation (ϕ) and rotation angles (γ), each cylinder or "branch axis" will have a different solar angle (Θ' and Θ'') with respect to the subtending cylinder (Θ). The influence of ϕ and γ on the Ap/A vs. Θ plots of a telome is shown in Fig. 3.

rationalized as being selectively advantageous as opposed to the horizontal growth of any comparable geometry. Vertical growth, however, imposes mechanical constraints. This will be addressed in the next section.

The telome.—A characteristic feature of many apical meristems is their capacity to produce branches or bifurcations. In the simplest land plant sporophytes, bifurcation of an axis results from the dichotomy of an apical meristem and the subsequent growth of the two resulting meristematic regions. The earliest vascular land plants apparently produced near equal bifurcations resulting in fairly uniform and isometric branching systems. Traditionally, a single bifurcation has been referred to as a "branched telome" (Zimmermann 1930), a diagram of which is shown in Fig. 2. The influence of bifurcation on the exposed surfaces of a plant to sunlight can be assessed if the telome geometry is reduced to its three cylindrical component axes, and if the divergence or bifurcation angle (ϕ) between the two distended axes is defined. In addition, since the two distended axes define a plane, the orientation of the telome to the solar angle, Θ , must be designated by means of a rotation angle, γ . From Fig. 2, the ratio between the projected

surface area and total surface area of a telome is given by the expression

$$\begin{aligned} Ap/A = \frac{\pi d}{4} & \left(\cos \theta - \sin \theta \sin \frac{\phi}{2} \cos \gamma \right. \\ & + \cos \theta \cos \frac{\phi}{2} + \sin \theta \sin \frac{\phi}{2} \cos \gamma \\ & + \cos \theta \cos \frac{\phi}{2} \Big) + bl(1 - \cos^2 \theta)^{1/2} \\ & + \left(1 - \sin^2 \theta \sin^2 \frac{\phi}{2} \cos^2 \gamma \right. \\ & + 2 \sin \theta \cos \theta \sin \frac{\phi}{2} \cos \frac{\phi}{2} \cos \gamma \\ & - \cos^2 \theta \cos^2 \frac{\phi}{2} \Big)^{1/2} \\ & + \left(1 - \sin^2 \theta \sin^2 \frac{\phi}{2} \cos^2 \gamma \right. \\ & - 2 \sin \theta \cos \theta \sin \frac{\phi}{2} \cos \frac{\phi}{2} \cos \gamma \\ & \left. \left. - \cos^2 \theta \cos^2 \frac{\phi}{2} \right)^{1/2} \left[3\pi \left(\frac{d}{4} + 1 \right) \right]^{-1} \right), \end{aligned}$$

where d and l are the diameter and length of each axial element of the telome. The area under the Ap/A curve (as a function of the solar angle, Θ , the bifurcation angle, ϕ , and the rotation angle, γ) can be calculated from this expression by means of a computer. The results for a branched telome consisting of three axes having a $l/d = 100$ is shown in Fig. 3. A large l/d value was selected to obviate the need to consider the Ap/A value of the interface between all three cylindrical axes (shown between dotted areas in Fig. 2).

It is clear from the geometry of a telome that for small bifurcation and rotation angles there will be considerable "self-shading" between the two side branches of the dichotomy. As the side branches are rotated (increasing γ -values), such that self-shading is reduced, the efficiency of intercepting sunlight at low and high Θ -values increases and the areas under the Ap/A curves concomitantly increase (Fig. 3). The highest value of $I(\phi)$ is where $\gamma = 90^\circ$ (telomic branches oriented perpendicular to the diurnal path of the sun) and $\phi = 180^\circ$ (the telome has a T-shaped geometry).

Vertical growth results in mechanical constraints on shape and the distribution of weight. A plant axis, oriented at some angle to the vertical, experiences internal compressive and tensile

stresses due to the bending moment imposed by the weight of the axis. Provided that these stresses do not exceed the tolerance limits of the axial tissues, the bending moment will not cause appreciable deformation. Continued apical growth of the axis will progressively increase the bending moment due to the accretion of new tissues. In contemporary plants, the stresses induced by indeterminate growth can be accommodated by (1) the alteration (increase) of axial cross-sectional area by means of secondary growth and (2) the alteration of the material properties of regions within an axis by means of "reaction wood." Plants lacking secondary growth, and therefore the capability of developmentally adjusting to increased internal stresses by means of (1) and (2), have been shown to reduce their bending moment by adjusting their total geometry such that internal stresses are minimized (Niklas and O'Rourke 1982). The available paleobotanical information on the earliest land plants indicates that the first land plants lacked secondary growth and the capacity to produce reaction wood. It is reasonable to surmise, therefore, that the stresses induced by orthotropic growth in vertical plants were minimized by means of adjusting the bifurcation angle (ϕ).

The relationship between ϕ and the bending moment of an axis, M , at the point to which it is attached to a subtending axis is given by

$$M = \frac{\pi}{\gamma} d^2 l^2 p g \sin \frac{\phi}{2}$$

where p is the mass weight of the axis and l and d are the length and diameter of the axis (cf. Fig. 2). Obviously, the optimal display of a telome's photosynthetic area ($\phi = 180^\circ$) maximizes the moment arm on its subtending axis. Although the relationship between the bifurcation angle (ϕ) and the moment arm (M) for a telome is clear-cut, a much more complex picture arises if the rotation angle (γ) is considered in conjunction with ϕ and M , particularly since γ has a profound influence on the efficiency with which photosynthetic surfaces are displayed with respect to the solar angle, θ . A computer simulation graphing the relationships among ϕ , M , γ , and l is given in Fig. 4A. Both Θ and ϕ are subsumed in the expression $I(\phi)$, which is the area under the Ap/A curve (as Θ varies from 0° to 180°). The resulting three-dimensional sur-

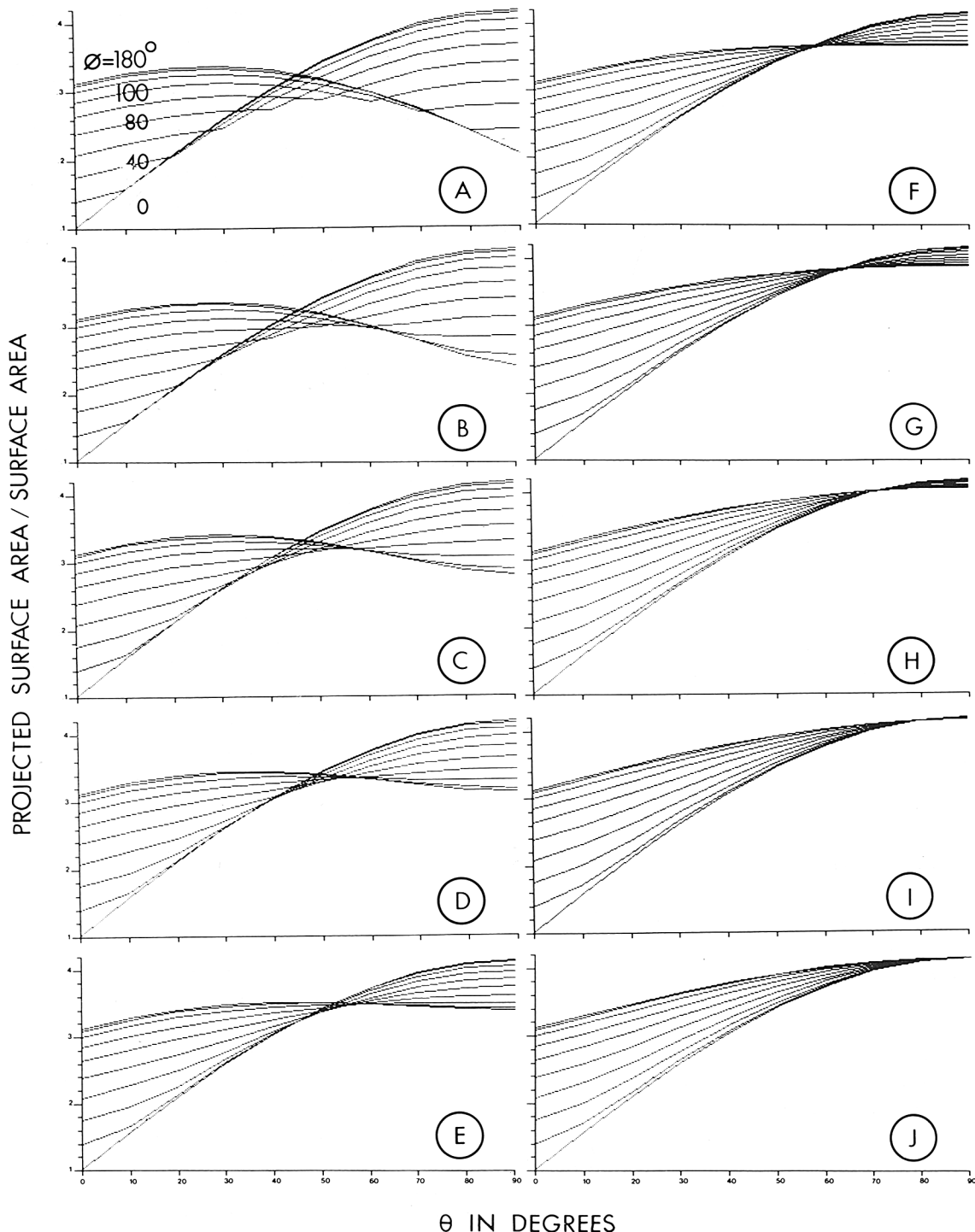


FIGURE 3. Computer-generated A_p/A vs. θ plots for a telome in which the bifurcation angle (ϕ) varies from 0° to 180° and the rotation angle (γ) varies from 0° to 90° (in 10° increments), A–J, respectively.

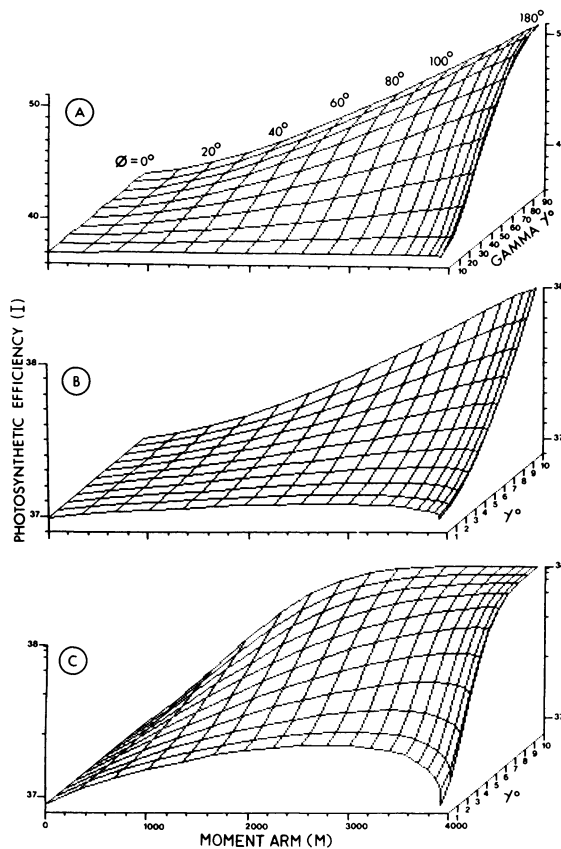


FIGURE 4. Computer simulation plotting multidimensional relationships among photosynthetic efficiency (I), moment arm (M), and rotation and bifurcation angles (γ and ϕ) for a single bifurcation (cf. Fig. 3). A, Plot based on $\gamma = 0^\circ - 90^\circ$ and $\phi = 0^\circ - 180^\circ$ (in 10° increments each) showing an increase in M as ϕ increases and an increase in I , as γ increases. B, Subregion of A ($\gamma = 0^\circ - 10^\circ$ in 1° increments) showing a depression in I for values of $0^\circ \leq \gamma \leq 4^\circ$ and $\phi \approx 100^\circ$. C, Expanded I axis augmenting the topography in the domain of $0^\circ \leq \gamma \leq 4^\circ$ and $\phi \approx 100^\circ$. Within this domain there exists a decline in photosynthetic efficiency (I), as ϕ and γ increase. Thus for $0^\circ \leq \gamma \leq 4^\circ$, I is maximized at $\phi \approx 100^\circ - 120^\circ$. For further details, see text.

face indicates that there exist two routes by which a telome's photosynthetic efficiency, given as $I(\phi)$, can be increased. The first route involves increasing the bifurcation angle (ϕ). However, this is only possible if the plant tissues involved can accommodate the rapidly increasing moment arm (M). The second route is to adjust the rotation angle of the telome (γ) with respect to the solar angle (Θ), perhaps through a phototropic (physiological) mechanism. This does not involve altering the mechanical properties of the telome, since $I(\phi)$ can be increased without changing ϕ , thereby keeping the moment arm constant. The

mechanical and physiologic solutions to maximizing photosynthesis are not mutually exclusive, and if operative together they increase the efficiency of displaying telomic surfaces to solar irradiance (Fig. 4B-C).

Higher-order branching.—An analysis of how photosynthesis and moment arm vary as a consequence of changing the geometry of a single bifurcation ("telome") is illustrative, but biologically trivial. The majority of vascular plant sporophytes are characterized by branching systems of a higher order than a single bifurcation, and may show large intra- and interspecific variation (Thornley 1977; White 1979). An extension of the "telomic" analysis to these more complex systems, therefore, requires a description of the geometric parameters that define the gross morphology of higher-order branching with attending modifications of notation.

Higher-order branching patterns were simulated by the computer program TREE BAS. All simulations were restricted to a maximum of 10 bifurcation events, N . The first formed or basal axis in each simulation was designated as nodal level 10 (i.e., $N = 0$) and all axes generated at nodal level 1 are terminal (i.e., $N = 9$). Branching patterns with varying degrees of bifurcation were simulated by defining the frequency of bifurcation, p (at each successively lower nodal level of bifurcation), according to the linear equation

$$p = \frac{8P_{n-(k+1)}}{N + k},$$

where $P_{n-(k+1)}$ is the probability of termination at the next generated (lower) nodal level and $N + k$ designates the previously generated nodal level. In all computer simulation runs p was varied from 0.0 to 0.9, with $p = 0.0$ (highest frequency of bifurcation) producing the most densely branched simulations and $p = 0.9$ (lowest frequency of bifurcation) yielding sparsely branched simulations. At the completion of simulations, branching order numbers were designated for each branching pattern. The ordering of branches conformed to the method first presented by Horsfield (1967; cf. Niklas 1982). Where bifurcation produces two axes of equal order number, the subtending axis receives an order number one higher than the two it subtends. The subtending axis to two unequal order

numbers is designated as one higher than the larger of the two distal axes, etc. This numbering system is illustrated for a structure with four orders of branching in Fig. 5.

Aside from varying the value of p , two additional geometric parameters must be specified before photosynthetic efficiency and total moment arm are computed for a particular branching pattern. These are the bifurcation and rotation angles, ϕ and γ (Fig. 6). Two categories of branching patterns can be generated by means of computer simulations, dependent upon the format in which ϕ_1 and ϕ_2 are varied: (1) isobifurcating branching systems resulting from $\phi_1 = \phi_2$ or $\phi_2 \neq \phi_1$, respectively, and (2) "pseudomonopodial" branching systems resulting from $\phi_1 = 0^\circ$ and $\phi_2 = 0^\circ\text{--}90^\circ$. The rotation angle, γ , specified for a higher-order branching pattern is unlike that previously described for a telome, since each successively higher bifurcation is not oriented normal to the true horizontal plane (compare Fig. 3 with Fig. 6A). Thus, γ is defined on the basis of an x - y coordinate system oriented normal to each subtending axis. The x - y position of one of the two axes resulting from a bifurcation is randomly selected from a range of values of which γ is the maximum value. The second axis is oriented 180° opposite the first. For $\gamma = 45^\circ$, the two axes may be positioned anywhere within 45° above or below the x -axis (Fig. 6B insert). For $\gamma = 90^\circ$, the two axes may be found opposite one another anywhere within the coordinate system, and for $\gamma = 0^\circ$ the axes lie along the x -axis. The consequences of this procedure are such that, for $\gamma = 0^\circ$, all branches are planated and diverge asymptotically to the horizontal plane for the entire branching system. For $\gamma = 90^\circ$, branching occurs in all directions and planation can only occur as a random consequence.

From the preceding, it is evident that photosynthetic efficiency (I), total moment arm (M), and I/M are dependent upon four geometric variables (p , γ , ϕ_1 , and ϕ_2). As a result, a conformational map showing how I , M , and I/M vary as a function of p , γ , ϕ_1 , and ϕ_2 is four-dimensional and difficult to visualize graphically. If ϕ_1 is set to equal some specified value ($\phi_1 = \phi_2$ for equal branching and $\phi_1 = 0^\circ$ for treelike branching), then a three-dimensional matrix can be defined with p , γ , and ϕ_2 as its three axes.

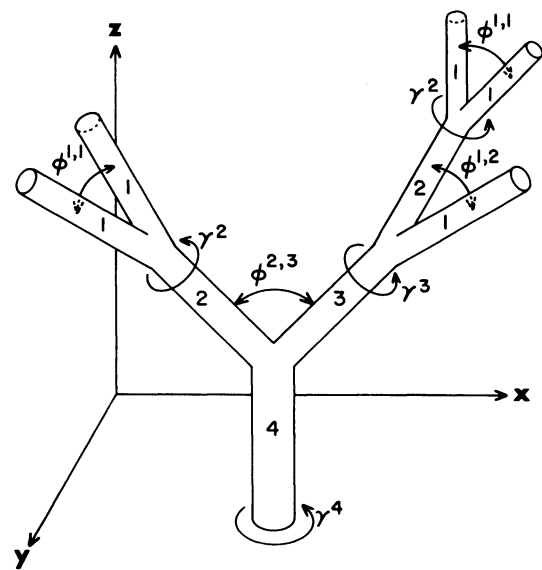


FIGURE 5. Notation for designating the various geometric features of an isobifurcating, three-dimensional, multiple-branched system. Terminal "branches" are designated order -1, while basipetal numbering provides for the recognition of a "main axis." Rotation angles (γ) are specified on the basis of the axis order number that is rotated. Bifurcation angles (ϕ) are specified on the basis of the two order numbers of the related bifurcating axes. A coordinate system (orthogonal arrows) provides a context in which rotation and bifurcation angles are related to one another and to the diurnal path of the sun. For further details, see text.

In the simulations to be presented, p is varied from 0.0 to 0.9 (in increments of 0.1), and γ and ϕ_2 are varied from 0° to 90° (in 10° increments). This procedure results in a three-dimensional matrix with 1×10^3 specified p , γ , and ϕ_2 coordinates and 20 bivariate planes—10 planes of p versus ϕ_2 (at $\gamma = 0^\circ\text{--}90^\circ$) and 10 planes of p versus γ (at $\phi_2 = 0^\circ\text{--}90^\circ$) (Fig. 7). For each set of coordinates, 10 branching patterns are simulated (1×10^4 branching patterns for each three-dimensional matrix). The values of I , M , and I/M given in the following simulations represent the averages for each set of 10 branching patterns that have been normalized on a scale from 0 to 9 (0 = low, 9 = high). Maximum I , M , or I/M scores for each bivariate plane through the matrix are identified by a black square. These maxima represent the position of the optimal branching pattern for each set of parameters that have been varied. For purposes of simplicity, only selected planes through the three-dimensional p , γ , and ϕ_2 matrix will be

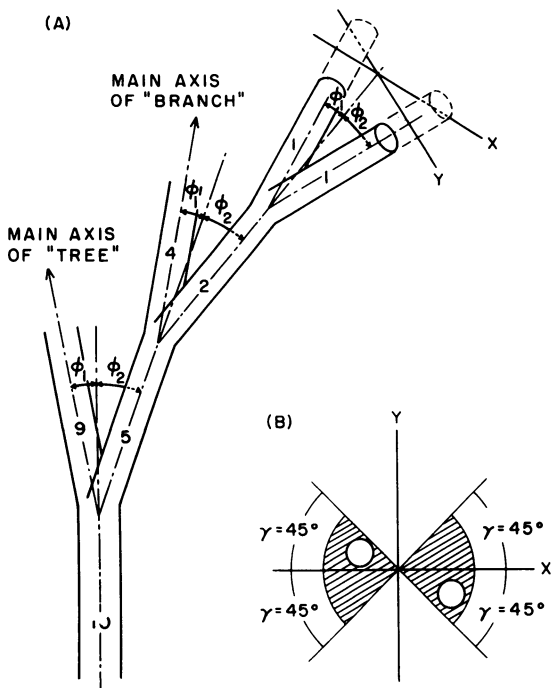


FIGURE 6. Notation for designating the various geometric features of a pseudomonopodial branching system. A, Branch order numbers are assigned as shown in Fig. 5. Unequal bifurcation angles (ϕ_1 and ϕ_2) are specified and result in the production of a "main tree" axis and "lateral branches." B, An extension of the longitudinal axis of each branch bearing two daughter branches defines the origin of a coordinate system (x - y) through which daughter axes are rotated. The rotation angle (γ) defines the extent through which bifurcate axes are rotated about the origin.

given. In addition, the geometry of representative branching patterns are given for selected regions in each simulation.

Isobifurcating (equal branching) systems.—The photosynthetic efficiency (I) and ratio of photosynthetic efficiency to total moment arm (I/M) for isobifurcating, higher-order branching systems ($\phi_1 = \phi_2$) are given in Figs. 8–9. Four planes were selected through the p , γ , and ϕ three-dimensional matrix: p versus ϕ for $\gamma = 90^\circ$, 60° , 30° , and 0° . Based on the position of I/M_{\max} , the optimal isobifurcating geometry is seen to be small in size (i.e., has a high probability of terminating bifurcation, $P = 0.9$) with large bifurcation angles ($\phi_1 = \phi_2 = 90^\circ$, or $\phi = 180^\circ$) (Fig. 8). The small size lessens the potential for self-shading, as does the large bifurcation angle and high degree of planation. The most inefficient branching patterns (lowest I/M value)

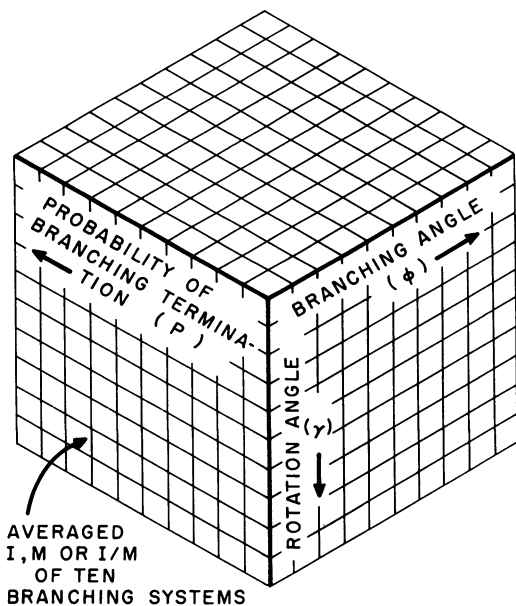


FIGURE 7. Three-dimensional matrix generated by varying the probability of terminating bifurcation (p), the bifurcation angle (ϕ), and the rotation angle (γ). Each axis has ten increments resulting in 1×10^3 specified p , γ , ϕ coordinate sets. Ten branching patterns are simulated for each specified p , γ , and ϕ coordinate set, and their averaged photosynthetic efficiency (I), total moment arm (M), or I/M computed.

in terms of maximizing I and minimizing M are produced when the probability of terminating bifurcation is low ($P = 0.0$) and when bifurcation angles are small ($\phi_1 = \phi_2 = 10^\circ$, $\phi = 20^\circ$) (Fig. 8). This yields erect plants with dense branching and strong self-standing, but with a low total moment arm. A localized high value for I/M exists for $p = 0.9$ and $\phi_1 = \phi_2 = 10^\circ$ ($\phi = 20^\circ$) and is geometrically represented by a sparsely branched, vertical branching geometry. For intermediate values of p and $\phi_1 = \phi_2$, a "bushy," divaricating geometry is produced (Fig. 8). As γ varies from 90° to 0° , branching geometries become planated (Fig. 8). Comparisons among the local I/M_{\max} for each of the four planes through the p , γ , and ϕ matrix indicates that I/M increases as γ approaches 0° . Thus, sparsely branched, planated geometries with large bifurcation angles have the highest I/M values for all the simulated, isobifurcating geometries.

Different optimal branching geometries are predicted on the basis of the same simulation if scored on the basis of I values (Fig. 9) instead of the trade-off between I and M (Fig. 8). Photo-

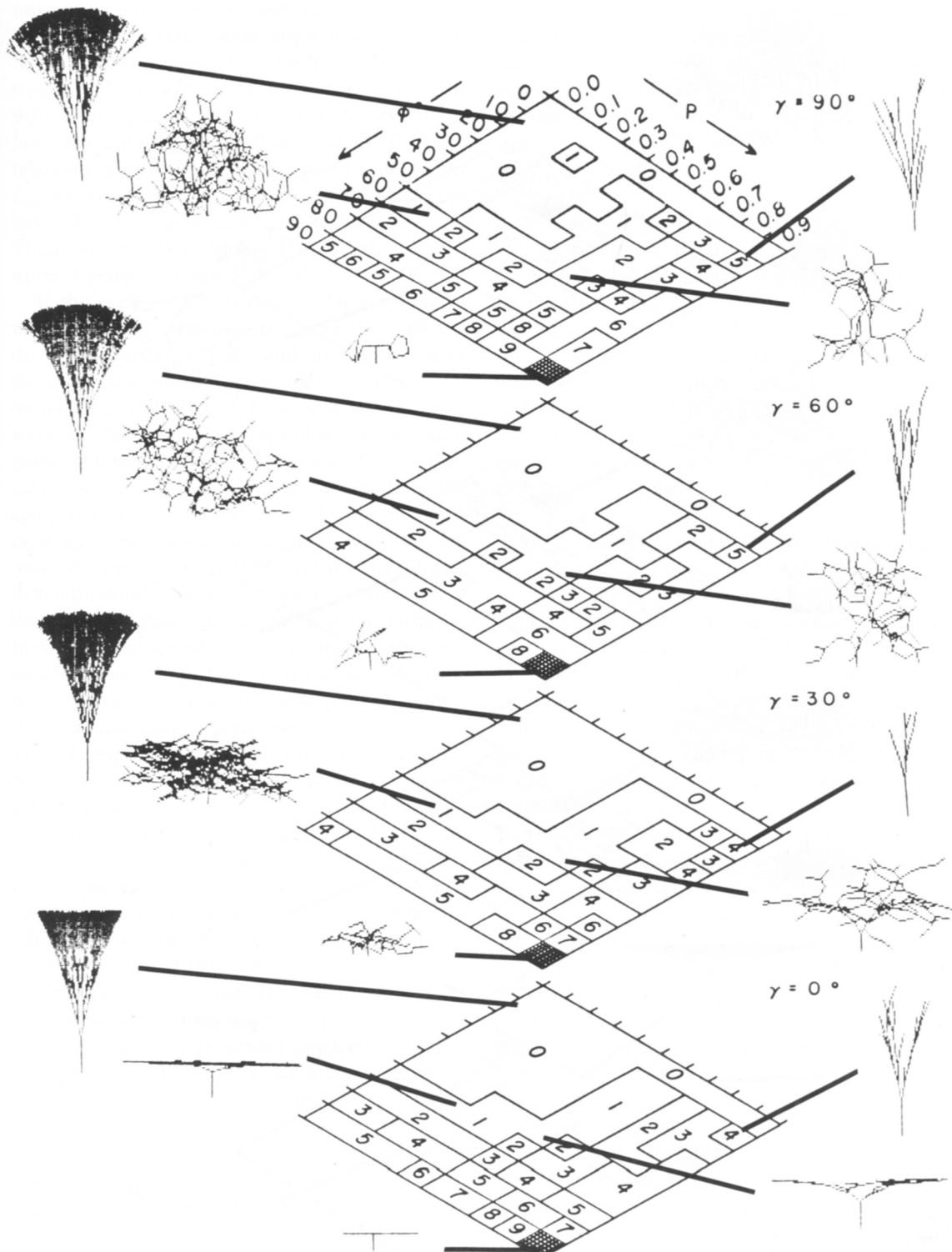


FIGURE 8. Four representative planes (p vs. ϕ for $\gamma = 90^\circ, 60^\circ, 30^\circ$, and 0°) through the p , γ , and ϕ three-dimensional matrix of isobifurcating branching systems. Values indicated for each region within each plane represent I/M averaged scores (0 = low, 9 = high, darkened area = I/M_{\max}). Representative branching patterns (seen in axial view) are given for selected regions.

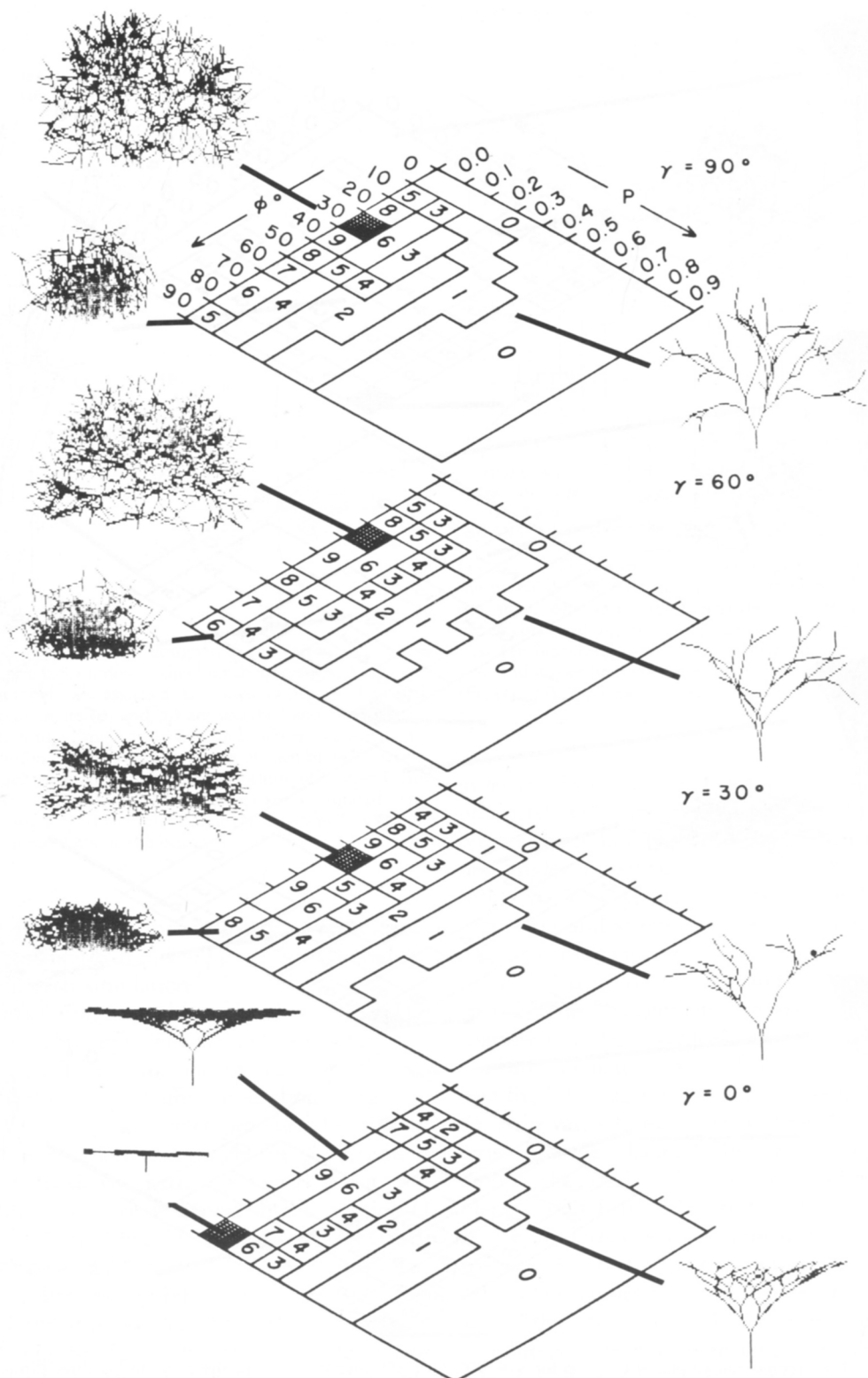


FIGURE 9. Four representative planes shown in Fig. 8. Data scored for photosynthetic maxima.

tosynthetic efficiency increases as the probability of terminating bifurcation approaches $P = 0.0$. Similarly, I increases when the bifurcation angle equals 30° – 40° (for γ -values between 30° and 90°). With planation ($\gamma = 0^\circ$), the optimal bifurcation angle equals 180° ($\phi_1 = \phi_2 = 90^\circ$). The relationship between the positions of I/M_{\max} and I_{\max} shown in Figs. 8 and 9 is explicable on the basis that I_{\max} generally corresponds to M_{\max} . Therefore, the branching geometry that maximizes I generally maximizes M .

If the early evolution of vascular land plants was dictated by selection pressures that favored the optimization of light and the reduction of the total moment arm, then the geometries corresponding to I/M and I maxima should have some similarities to the morphology of early land plants. However, the extent to which early vascular plant morphologies are reflected in the computer analyses is influenced by the former's capacity to withstand mechanical stresses (which may obviate the requirement to minimize M) by developmentally adjusting such parameters as branching and rotation angles and the termination of apical growth. If it is argued that the earliest land plants had to minimize M while maximizing I and that the subsequent evolution of structural tissues permitted plants to maximize I even with a substantial moment arm, then plant morphology should have undergone a transition from those shown by I/M_{\max} (Fig. 8) to those shown by I_{\max} (Fig. 9). This trend would correspond to a transition from a diminutive, sparsely branched plant to a larger, more vertical, and robustly branched morphology. In addition, computer simulations optimizing I or I/M are planated (Figs. 8–9).

The earliest vascular land plants, such as *Cooksonia*, were small, sparsely branched, lacked tapering axes, and possessed apparently slender supporting vascular traces. As a consequence of their anatomy and morphology an I/M optimization strategy seems reasonable. The correspondence between the morphology of *Cooksonia* and that of the simulated branching patterns with I/M_{\max} is reasonably good and provides some basis for accepting the biological relevancy of the trends seen in Fig. 8. *Cooksonia* and other Upper Silurian and Lower Devonian land plants had three-dimensional branching and apparently lacked the capacity to planate. Of interest in this

regard are the consequences of mechanical stresses incurred by the indeterminate growth of vertical axes. Given a limited capacity to sustain vertical growth, induced compression and tensile stresses would cause a repeatedly bifurcating system to reapportion vertical axes into a horizontal position (Niklas and O'Rourke 1982). Thus, even though "planation" of vertical axes may have not occurred due to direct developmental control, it would result from the mechanical failure of vertical axes that continued to grow. This would have "planated" the bulk of a *Cooksonia*-like plant's branching system onto the substrate, producing a rhizomatous branching system with short vertical axes.

If the unrolling ball of yarn analogy is correct, then the "telomic" analysis of how I varies as a function of γ and ϕ would be appropriate for the vertical (= orthotropic) axes of the plant. Thus Fig. 4 and Figs. 8–9 can be considered in tandem, with each vertical "telome" shown in Figs. 8–9 having the properties of I shown in Fig. 4.

With subsequent anatomical variation (e.g., the evolution of more robust vascular and structural supporting tissues and/or the appearance of axial tapering), the I/M optimization strategy could be replaced by one favoring photosynthetic efficiency. The production of a three-dimensional and overtopped branching pattern allows for a more photosynthetically efficient plant than that produced by a planated, but essentially two-dimensional branching pattern structure sprawled over the substrate. Lower Devonian vascular plants, such as *Rhynia*, show much more extensive vertical growth than Upper Silurian taxa such as *Cooksonia*, and may represent the transition from a branching geometry that optimizes I/M to one that optimizes I .

With the transition from an I/M to I maximizing strategy, a "bushy" three-dimensional branching pattern would be predicted (Fig. 9). Continued apical growth of such a system, however, results in a decreasing photosynthetic efficiency due to self-shading. As seen from computer simulation, self-shading can be reduced and I maximized by adjusting the rotation angle such that planation occurs (Fig. 9). From a purely geometric consideration, however, planation has its own structural limits for a plant with indeterminate growth, that is, at some point the distal axes of a planated, branching geometry

will impose mechanical stresses exceeding the carrying capacity of the tissue and cause the structure to fail under the influence of gravity. This impasse can be resolved by adjusting the bifurcation angle such that it is not symmetric ($\phi_1 \neq \phi_2$). Once this is achieved, pseudomonopodial branching will occur, that is, some branches will overtop others resulting in a tree-like branching geometry.

Pseudomonopodial (treelike branching) systems.—Figures 10–11 show the variation of I/M for monopodial branching ($\phi_1 = 0$) in six planes through the three-dimensional p , γ , and ϕ_2 matrix (i.e., p vs. ϕ_2 for $\gamma = 0^\circ$, 45° , and 90° ; and p vs. γ for $\phi_2 = 10^\circ$, 45° , and 90°). I/M is seen to increase as p and ϕ_2 increase (i.e., the extent of lateral branching, p , decreases toward the top of the tree and lateral branches are borne at greater angles, ϕ_2 , to the main axis), and as γ decreases (lateral branches become planated). The shape of branching patterns conforming to this “optimizing” solution is similar to the pagoda-like tree architecture of some conifers (e.g., *Picea glauca*). Another, less efficient solution to maximizing I/M (i.e., a localized region of I/M maximization) is seen when ϕ_2 is kept relatively small (10° – 20°), p is kept large (acropetal diminution in the growth of laterals), and γ is large (branching is nonplanated). The shape of branching patterns conforming to these conditions is similar to that seen in some extant pteridophytes (e.g., *Psilotum nudum*). As γ decreases ($\gamma = 0^\circ$), a region of low I/M values gradually expands between the *Picea*- and *Psilotum*-like branching patterns. Branching patterns characteristic of this “intermediate” region are similar to those seen in many arborescent flowering plants (e.g., *Quercus*). Such treelike architectures have extremely high total moment arms and low photosynthetic efficiencies. The I/M matrix produced by varying p , γ , and ϕ_2 when $\phi_1 = 0^\circ$ may be divided into three regions, each characterized by a type of branching geometry that has a generalized botanical analogue—some pteridophytes (= *Psilotum*-like),

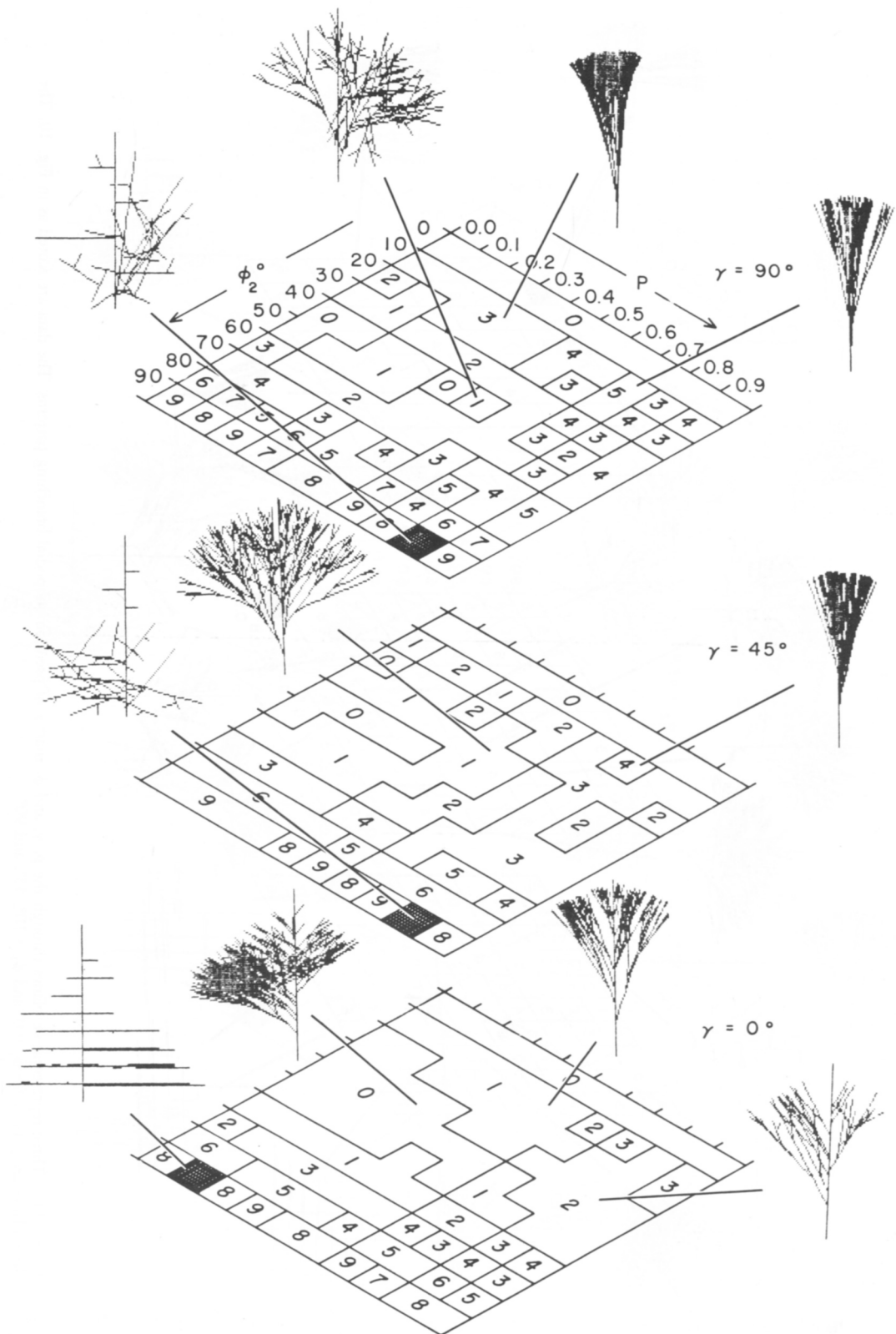
gymnosperms (= *Picea*-like), and angiosperms (*Quercus*-like). Only two of these three regions appear to optimize I/M (*Psilotum*- and *Picea*-like). If I -values are computed for the p , γ , and ϕ_2 matrix, the positions of optima are seen to conform to the *Quercus*-like branching patterns (Fig. 12). The *Psilotum*-like branching patterns have the lowest I -values, and the *Picea*-like branching patterns have intermediate I -values. Botanical analogues to the *Quercus*-like branching patterns are seen in arborescent flowering plants, characterized by possessing secondary vascular cambia and reaction wood which can geometrically compensate for mechanical stresses by increasing cross-sectional surface area in older stems and by changing the material properties of wood. In addition, flowering trees have their megaphylls generally concentrated on younger branches, and as such, their photosynthetic structures are peripheral (reducing self-shading) and have large surface areas. Under these circumstances it is reasonable to assume that the constraints on their branching patterns are best modelled by optimizing I rather than I/M , since anatomical features (secondary cambia and reaction wood) can minimize M .

Another perspective on the extent to which variations in branching geometry maximize I or I/M is gained by converting absolute values into percentages relative to I/M_{\max} or I_{\max} (Fig. 13). Except for extremely low values of ϕ_2 (0° – 10°), all of the values of I/M are between 60% and 90% of the I/M_{\max} values, indicating that most of the simulated branching patterns are relatively efficient in their photosynthetic capacity versus moment arms trade-off. The gain in photosynthetic capacity attending geometric alterations in branching patterns, however, cannot be converted into an actual physiologic gain. Hence the distinction between I/M values that are 70% or 80% of I/M_{\max} may be greater or less than indicated by percentage values.

Photosynthetic efficiency as a function of varying Θ and self-shading.—The computer simulations presented in Figs. 8–13 are based on calculating I for a single, specified orientation to

FIGURE 10. Three representative planes through the p , γ , and ϕ_2 matrix of pseudomonopodial branching patterns. The data are scored (0 = low to 9 = high) for I/M values (maxima shown as darkened areas). The three planes are p vs. ϕ_2 for $\phi_1 = 0^\circ$ and $\gamma = 90^\circ$, 45° , and 0° .





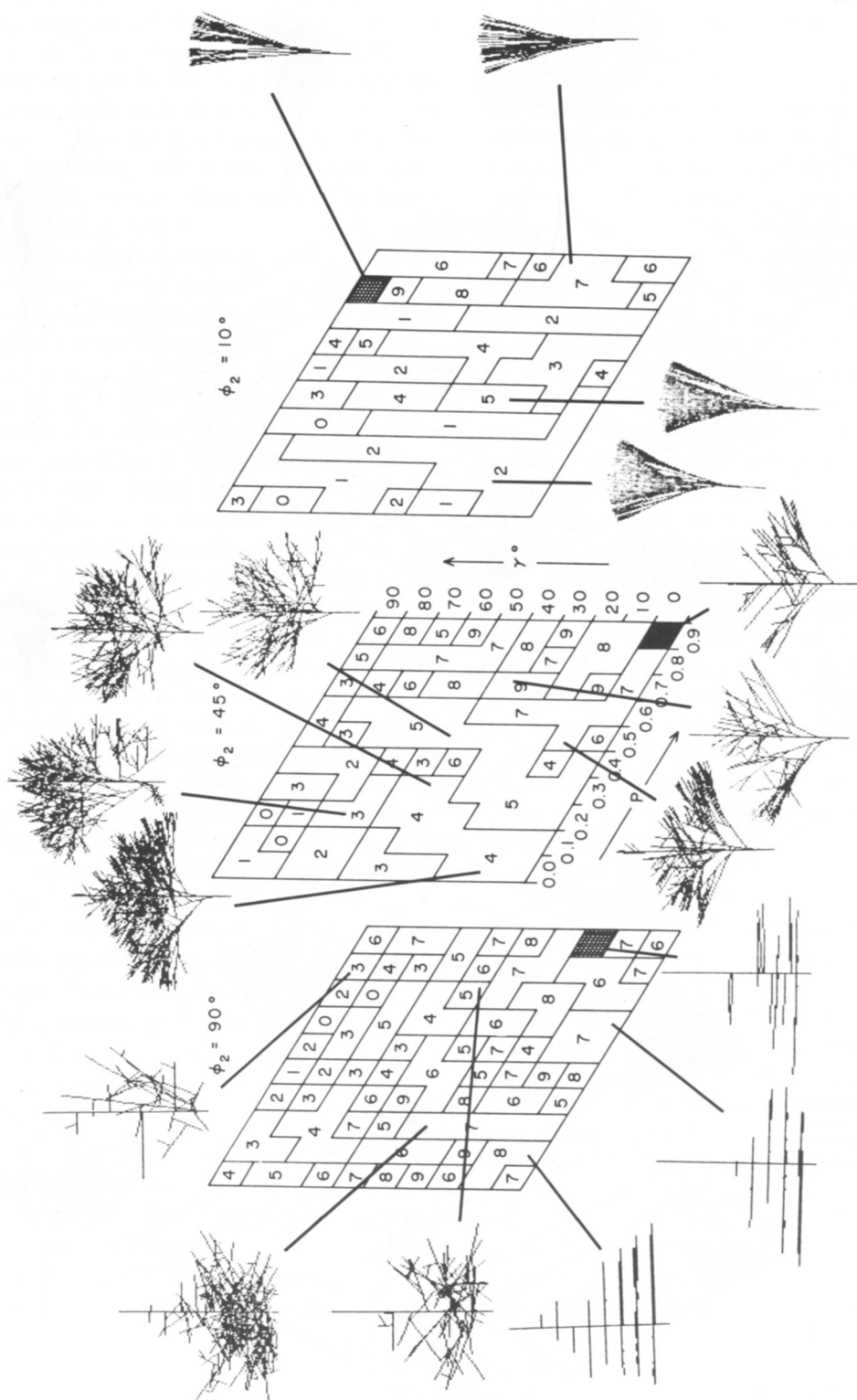


FIGURE 11. Three representative planes through the p , γ , and ϕ_2 matrix of pseudomonopodial branching patterns. The data are scored as in Fig. 10. The three planes are p vs. γ for $\phi_1 = 0^\circ$ and $\phi_2 = 10^\circ$, 45° , and 90° .

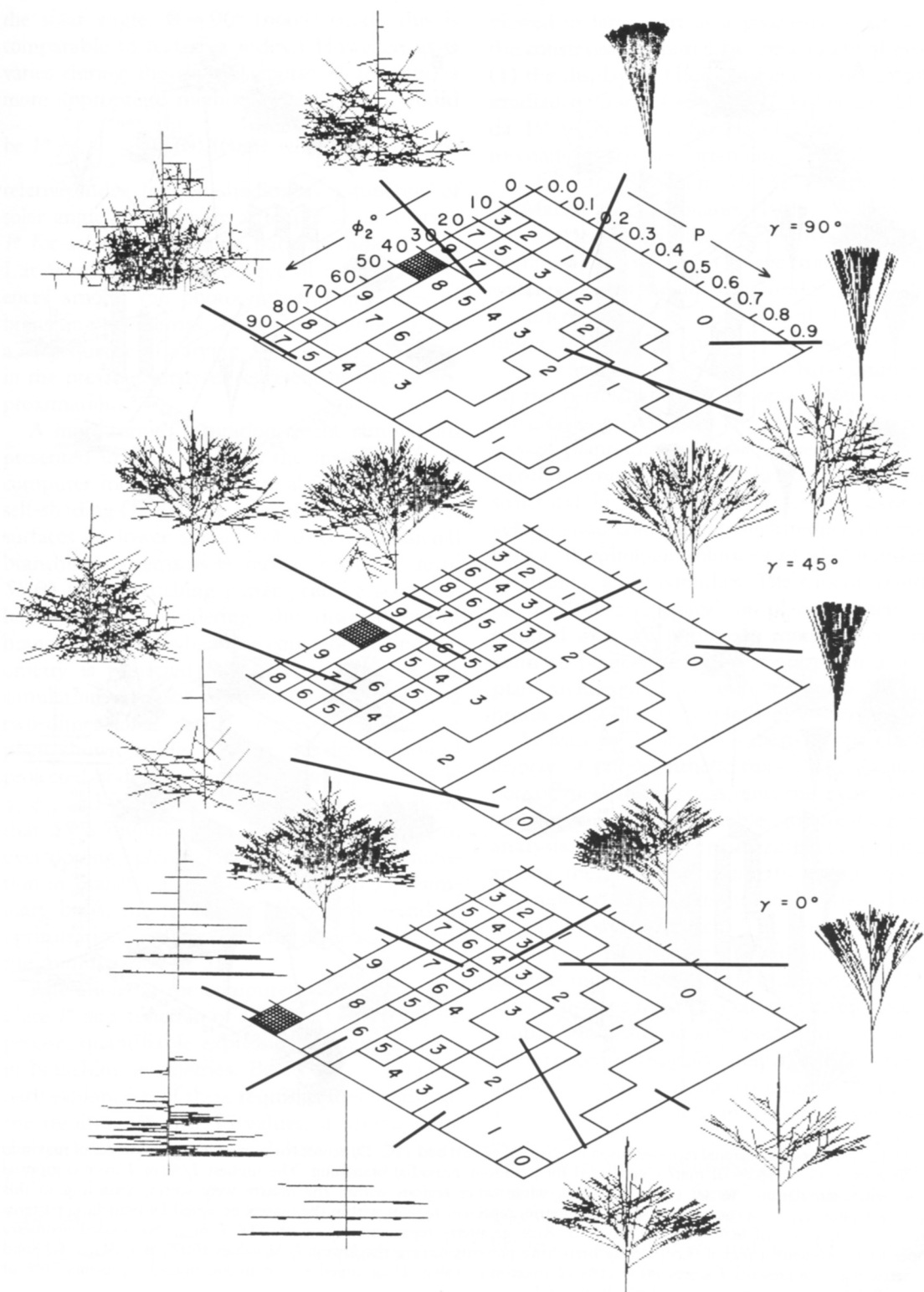


FIGURE 12. Three of the six planes shown in Fig. 10 (p vs. ϕ_2 for $\phi_1 = 0^\circ$ and $\gamma = 90^\circ$, 45° , and 0°), scored for I (0 = low to 9 = high, maxima in darkened areas).

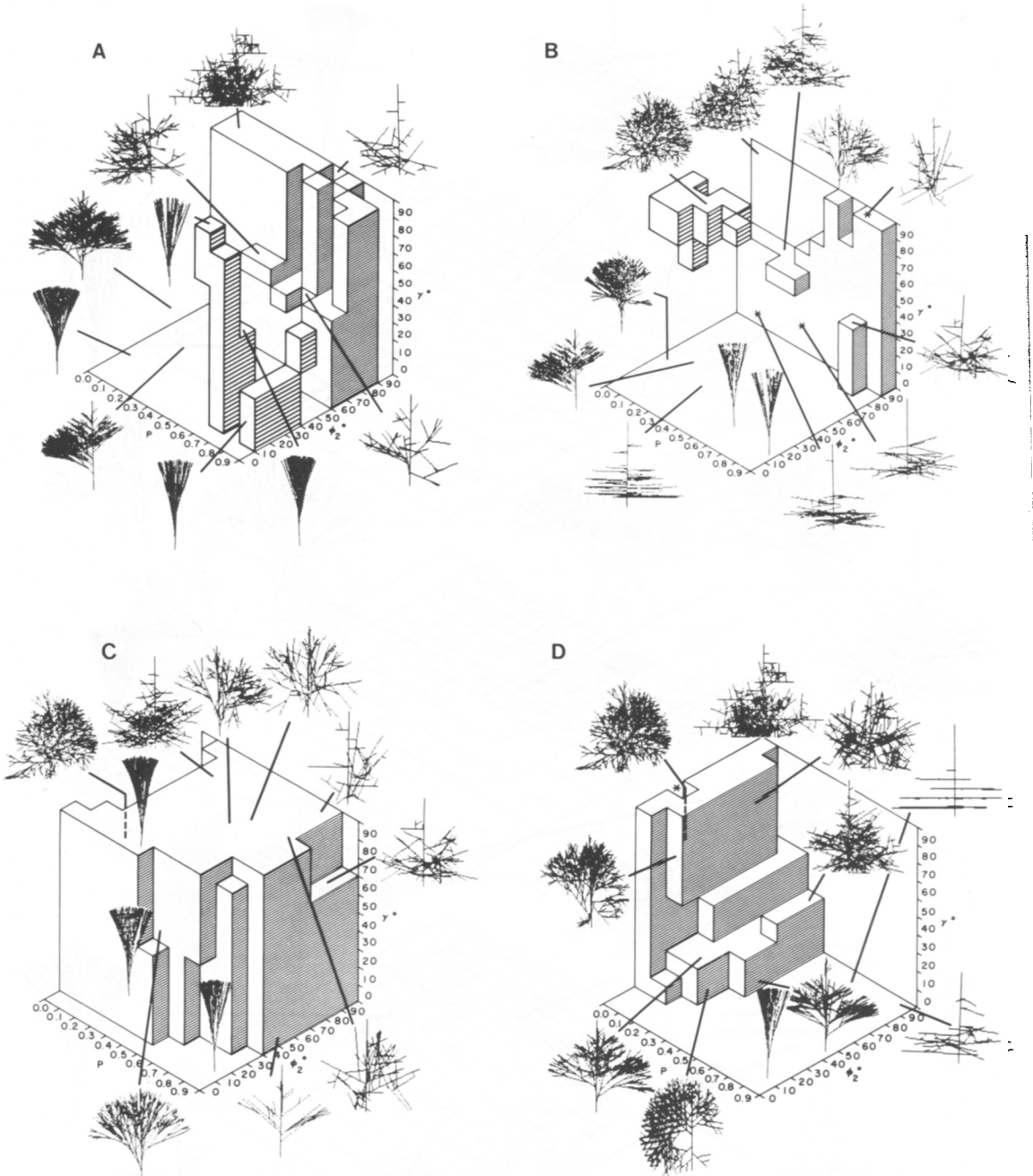


FIGURE 13. Three-dimensional representation of the I/M (A-B) and I (C-D) scores (converted into percentages of maxima) for the ρ vs. γ vs. ϕ_2 ($\phi_1 = 0$) matrix generated for pseudomonopodial branching. The highest I/M or I score computed in the entire simulation was set equal to 100%, while other regions within the matrix were scores, according to this maximum value. A, Solid three-dimensional geometries represent regions within the matrix occupied by branching patterns that have I/M scores of 80% of the I/M_{\max} . B, Rear geometry represents region of 90% I/M_{\max} . Suspended geometry (upper left) represents a region occupied by branching patterns having the lowest I/M values (60% of I/M_{\max}). C, Solid geometric region represents I scores 80%–70% of maximum value. Unoccupied region in foreground represents 70% of I_{\max} . D, Solid geometry representing 90%–100% of I_{\max} .

the solar angle, $\Theta = 90^\circ$ (noon) (note, this is comparable to leaf area index.) However, as Θ varies during the diurnal course of the sun, a more appropriate method of simulation would

$$\text{be } I^* = \int_{0^\circ}^{180^\circ} SS(\Theta)I(\Theta)d\Theta \text{ where } SS(\Theta) \text{ is the}$$

relative index for self-shading as a function of solar angle. Preliminary attempts at calculating I^* for selected branching patterns indicate that I at $\Theta = 90^\circ$ is representative of relative differences among the photosynthetic efficiencies of branching geometries. Thus the variation of I as a consequence of varying p , γ , ϕ_1 , and ϕ_2 given in the previous analyses represent first-order approximations.

A more serious limitation to the simulations presented in Figs. 8–13 is the inability of the computer model to calculate absolute values of self-shading ($SS(\Theta)$), i.e., the projection of upper surfaces on lower surfaces of three-dimensional branching patterns as Θ varies.¹ An estimate of $SS(\Theta)$ for a branching pattern can be achieved, however, by considering the distribution of branching nodes when the entire branching geometry is projected in the axial plane of the simulation, i.e., the distribution of nodes on a two-dimensional surface representing the x - y plane shown in Fig. 5. Since the distribution of projected nodes is a geometric consequence of p , γ , ϕ_1 , and ϕ_2 , variation exists, analyses indicate that SS is minimized as I is maximized due to overtopping, planation, and acropetal diminution in branching frequency. Thus on a preliminary basis, the geometric alterations attending optimization of I or I/M are compatible with the minimization of SS .

Alterations in the computer program to simulate I^* as a function of SS are necessary to give precise, quantifiable expressions of optimization in branching geometries. Based on our preliminary exploration of these requisite alterations and the resulting I^* and SS values, it appears that the general trends reported here will be reinforced.

Discussion

The morphology of a terrestrial plant may be

viewed in large part as a geometric solution to the constraints imposed by three essential tasks: (1) the display of photosynthetic tissues to solar irradiance (Gates 1965, 1970; Fisher and Honda 1979; Nobel 1980, 1981, 1982); (2) the mechanical stresses attending vertical growth (Archer and Wilson 1973; Honda 1971; McMahon and Kronauer 1976; Wilson and Archer 1977; Niklas and O'Rourke 1982; Whitney 1976); and (3) the translocation of water and metabolites (Shinozaki et al. 1964; Zimmermann 1978; Honda et al. 1981; Tomlinson 1983). The optimal performance of any one of these tasks imposes structural limitations on the performance of the others and, since all three tasks are essential for survival, the geometry of plant form may be viewed as an architectural compromise. In addition to the inherent structural limits to plant form, there exist developmental constraints which reduce the number of morphologic solutions to photosynthesis, mechanics, and hydraulics. The superimposition of this "phytic legacy" on plant geometry has resulted in a discontinuous morphologic spectrum to plant structure, recognized in a set of plant architectural models ("Baupläne") (Tomlinson and Gill 1973; Hallé et al. 1978).

At least in theory, resolutions to the efficient display of photosynthetic tissues, the equilibration of mechanical stress, and the hydraulics of translocation are amenable to mathematical analysis. As such, optimizing compromises among the attending geometric constraints can be predicted. There are, however, obvious limitations to this approach. The number of variables, both physiologic and morphologic, are so great as to preclude closed-form solutions. Thus some variables must be excluded or grouped, or simplifying assumptions must be made. Each of these procedures immediately jeopardizes the biological relevancy of the conclusions from such a study. Similarly, it is incumbent upon theory to be gauged by empirical observation, which in this case requires knowledge of developmental constraints on plant form. To be useful, therefore, theoretical assessments must be initially limited to a few cases and amenable to some test.

The present study represents an attempt to predict which architectural solutions to photosynthetic efficiency and consequent moment arms are more efficient than others, and is restricted

¹ Self-shading and shading from nearby plants were probably critical factors influencing the evolution of treelike branching.

in the scope of its analysis to plant morphologies of extremely simple geometries, that is, spheroids and bifurcating cylindrical elements. The parameters considered were restricted to the projected to total surface area ratio (as a gauge of photosynthetic efficiency), and such features of branching geometry as bifurcation and rotation angles and the frequency of bifurcation. Based on these parameters, computer simulations of possible permutations were generated. Owing to the relatively simple geometries (= "morphologies") that were simulated, and to the assumption that no profound physiologic differences existed among these geometries, the biological relevancy of this study is restricted to the early evolution of the land flora. Limited extrapolation to more recently evolved plant morphologies is possible but lacks any guarantee that the organisms in question are physiologically comparable.

Effectively, the objective of this study was to predict all mathematically conceivable solutions, determine the relative efficiency of each, determine trends that lead toward greater efficiency, and to see if these trends are discernable in the fossil record—the ultimate arbitrator of theory. Of interest are (1) the computer-simulated "morphologies" that have no discernible botanical analogues, since these may reflect developmental solutions that cannot exist in nature, and (2) the relative efficiency of simulated forms that do have botanical analogues, since this may afford a crude basis for assessing the selective advantages to broad trends in plant evolution.

Based on computer analyses, a number of geometric changes are seen to enhance the photosynthetic efficiency of a plant: (1) a transition from diffuse growth to localized (apical) growth; (2) repeated bifurcation of cylindrical elements ("axes"); (3) orthotropic orientation of axes; (4) adjustment of bifurcation and rotation angles toward the diurnal path of the sun; (5) adjustment of the frequency of bifurcation, resulting in the production of an "overtopped" branching pattern; (6) a tendency to produce a "main" vertical axis, bearing "lateral branching" systems, that acropetally decrease in size; (7) a tendency to "planate" lateral branching systems; and (8) the support of lateral, planated branching systems at right angles to the main vertical axis. Inherent to these seven optimizing geometric adjustments is a predicted tendency toward a more pro-

nounced vertical aspect. These trends are diagrammatically summarized in Fig. 14.

Of the eight trends predicted by computer simulation to enhance photosynthetic efficiency and minimize total moment arm, all are detectable as major trends in early land plant evolution. The first vascular land plants were the rhyniophytes, typified by *Cooksonia*, *Rhynia*, and presumably *Steganotheca* (whose status as a tracheophyte is as yet unconfirmed). The rhyniophytes are characterized as small, simple plants with more or less equally branched axes (e.g., Fig. 14A). Based on petrifications of *Rhynia*, the branching system of these plants had limited vertical growth and was three-dimensional. The rhyniophytes are believed to have been ancestral to the trimerophytes, which in turn are believed to have been the ancestral plexus from which all subsequent vascular land plants, with the exception of lycopods, evolved. The trimerophytes, are best known on the basis of three genera (*Psilotophyton*, *Trimerophyton*, and *Pertica*), and are characterized by unequal branching to pseudo-monopodial or treelike branching systems (e.g., Fig. 14C–D). Based on reconstructions, the trimerophytes had evolved main vertical axes that bore less robust or extensive "lateral" branching systems. The branching geometry in these plants appears to be three-dimensional, with lateral systems having varying extents of determinate growth. By Middle to Upper Devonian times, a number of taxa appear to have evolved lateral branching systems that were planated (e.g., *Cladoxylonida*, *Rhacophytopsida*, and *Archeopteridales*) as well as the megaphylls (presumably derived from lateral, webbed branching systems) seen in various filicopsids (Fig. 14E).

Underlying the trend toward the evolution of a main vertical axis with lateral, planated appendages is another toward greater vertical (orthotropic) growth. It is evident that starting with *Cooksonia* ($Diam_{max} = 0.3$ cm), larger plants progressively evolved until by the end of the Devonian, *Archaeopteris* (with *Callixylon* wood) was more than a meter in diameter (Zimmermann 1930; Chaloner and Sheerin 1979). Although the corresponding height of a plant cannot be directly calculated from the girth of its basalmost axis, diameter is correlated with height. As such the paleobotanical data indicate that trees of substantial vertical posture had appeared

within 50 Myr of the occurrence of the first vascular plants.

Traditional paleobotanical speculation on the evolution of increased vertical aspect has emphasized the selective advantage of gaining greater access to light and of greater effective ranges for spores or propagules borne on aerial branches (Bower 1935; Zimmermann 1930; Banks 1968, 1972; Chaloner and Sheerin 1979). It is of interest that the tendency toward greater height can be predicted (and computer simulated) solely on the basis of optimizing the photosynthetic display of tissues and minimizing the total moment arm of a branching system. Based on the simulations presented here, it is not necessary to consider reproductive effects in order to predict an evolutionary increase in plant height.

The physical constraint of hydraulics on plant form has not been rigorously approached in this study. This is due to a general lack of understanding concerning the relationship between the gross morphology of branching (e.g., bifurcation angle, tapering of axis girth) as it directly relates to the flow rates of water and metabolites. It is reasonable to assume that anatomical factors (e.g., stellar morphology, and length, width, and number of tracheids and/or vessel members) will play a critical role in hydraulics (Zimmermann 1978). However, as Tomlinson (1983, p. 147) points out that, for a plant to grow tall, "its upper axes must be favored in the distribution of the water supply" and "the early replacement of equal dichotomy . . . by some kind of controlled lateral branching may well be the first morphological manifestation of this simple physiologic requirement." Murray (1927) determined a linear relationship between the logarithm of the circumference of a tree, branch, or leaf stem, and the logarithm of the weight above the point at which the circumference was measured. Based on a previous analysis of optimal bifurcation angles for blood flow in arteries (Murray 1926a,b,c), he attempted to define the optimal bifurcation angles for water flow in plant branching systems using the exponent of a linear regression of weight versus circumference and the ratios of the subtending and bifurcating axes. Given an empirically determined linear regression exponent of 2.5 for a variety of trees (aspen, butternut, hickory, oak, ash, maple, cedar, hornbeam, and beech), Murray (1927, p. 728) de-

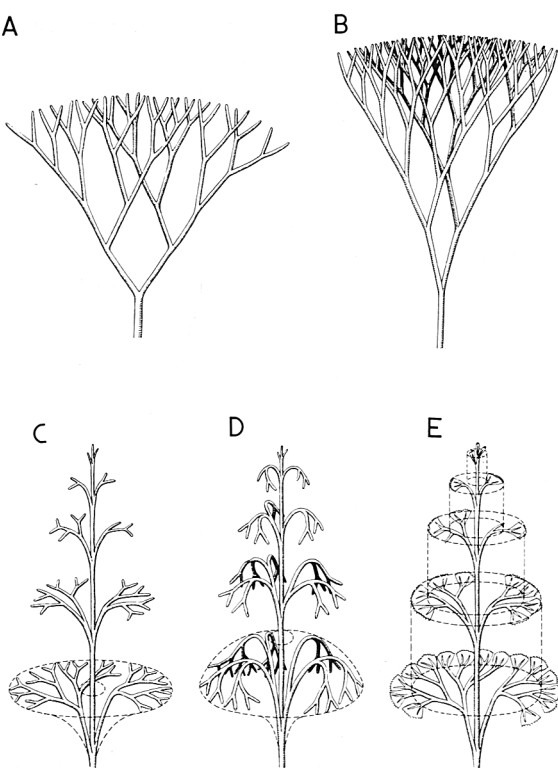


FIGURE 14. Geometric patterns of branching predicted by computer to successively increase photosynthetic efficiency. A, Isobifurcating ($\phi_1 = \phi_2$) branching displays photosynthetic axes in three dimensions. B, Limits to isobifurcation occur due to self-shading require adjustment of bifurcation angles such that $\phi_1 \neq \phi_2$. C, D, Overtopping and planation of branching system minimize self-shading.

duced an optimal bifurcation angle of 59° for water flow when the circumferential ratio of two bifurcating branches equals one. We have measured bifurcation angles between the axes of selected vascular plants and compared these angles with those predicted for optimal flow rates given the circumferential ratios of parent and daughter axes. In most cases there exists a reasonable correlation (unpublished data). Murray's (1927) equations would predict that for a plant lacking secondary growth (axes having a relatively uniform girth throughout the plant body), the optimal bifurcation angle should be very small. As the parent-axis circumference increases in proportion to the two daughter-axes circumferences, the optimal bifurcation angle should become larger. Similarly, as one of the two daughter axes becomes larger in girth with respect to the other, the optimal bifurcation angle likewise increases.

The maximum predicted bifurcation angle for a lateral branch on a main axis is 90°. Thus, optimizing trends for flow through branches correspond with optimizing trends in the display of photosynthetic tissues to incident solar irradiance.

Valid measurements of bifurcation angles observed in compression fossils are compromised by potential distortion during preservation. However, some fossil taxa show remarkably consistent bifurcation angles for a given order of branching (H. P. Banks and S. Scheckler, pers. comm. 1983). In general, the angles between compressed axes of Late Silurian to Devonian vascular plants increase as the parent-axis girth increases. With the advent of treelike morphologies, lateral branches of frondlike branching systems approach a 90° insertion into the main "trunk" or stem. Since this trend is predicted to optimize both photosynthesis and translocation, the relative contribution of each cannot be assessed. What is germane, however, is that both trends have nonantagonistic geometric solutions.

The relevancy of Murray's (1927) simple hydraulic model must be questioned, however, despite the conformity between its predictions and the fossil record. Differences between arteries and xylem tissue components (tracheids and vessels) are profound. Blood vessels are closed systems, consist of elastic tubes, and have pulsatile flow with Reynolds numbers four orders of magnitude greater than those of a xylem vessel (e.g., the human aorta has a Re of 2,000, while that of a xylem vessel is 0.02). In an analysis of phloem fluid dynamics, Rand and Cooke (1978) and Rand et al. (1980) showed that Poiseuille's law (used in Murray's [1927] treatments of blood and water flow) underestimated pressure drops through a series of cylindrical sieve tubes by a factor of two (cf. Rand 1983, pp. 31–32). Although these studies were based on the relatively unrealistic axisymmetric case of a single pore between the sieve tubes, it is obvious that the fluid dynamics encountered in blood vessels and xylem vessels are quite different (e.g., slow quasi-steady, viscous flow in a rigid-tube model is appropriate for xylem tissues but totally inappropriate for arteries). It is obvious that much more needs to be known about the fluid dynamics of plants before hydraulic constraints can be integrated into the analysis of plant form.

The fossil record of plant evolution represents the morphologic outcomes of a protracted series of "experiments" which "attempted" to resolve the constraints inherent to the geometry of structure and function. In large part, this record reflects the success of reproductive strategies; however examination of the vegetative morphology and anatomy of fossil plants gives clues as to how plants solved the display of photosynthetic tissues, the mechanics of vertical growth, and fluid dynamics. Common to the morphology of most vascular plant lineages was the evolution of leaves borne on vertical, supporting axes that bifurcated to eventually produce treelike structures. Most plant groups are seen to have evolved secondary growth, thereby increasing the girth of supporting axes with a commensurate increase in the capacity to withstand compressional and tensile stresses. The morphology and anatomy of "leaves," "branches," and "main trunk" differ substantially among the various vascular plant groups and reflect different developmental pathways to the solution of photosynthesis, mechanics, and hydraulics. (The evolution of microphylls and megaphylls reflects two different morphological responses to selective pressures favoring increased photosynthetic surface area.) The fossil record thus provides a broad empirical survey of botanical "experiments"—some of which were more successful than others as gauged by fossil species durations, diversifications, and extinction rates. It should be noted that vascular plant evolution in terms of morphology and anatomy represents only half the picture to the solution of vegetative growth. The nonvascular embryophytes (mosses and liverworts) have gone through their own, often unique, evolutionary experimentation—sometimes with convergent results (e.g., phyllids, bifurcating axes, and conducting cell types). The present study represents an initial and still crude attempt to determine the inherent constraints and selective advantages to evolutionary changes in plant form.

Acknowledgments

The authors wish to thank Drs. Rolf Borchert (University of Kansas), Jack Fisher (Fairchild Tropical Garden), Thomas Poulson (University of Illinois at Chicago Circle), Bruce Tiffney (Yale University), and Barry Tomlinson (Harvard

University) for their comments and suggestions made on an early draft of this paper.

Literature Cited

- ANDERSON, M. C. 1964. Studies of the woodland light climate. I. The photographic computation of light conditions. *J. Ecol.* 52: 27-41.
- ARCHER, R. R. AND B. F. WILSON. 1973. Mechanics of the compression wood response. II. On the location, action, and distribution of compression wood formation. *Plant Physiol.* 51:777-782.
- BANKS, H. P. 1968. The early history of land plants. Pp. 73-107. In: Drake, E. T. ed. *Evolution and Environment*. Yale Univ. Press; New Haven.
- BANKS, H. P. 1972. The stratigraphic occurrence of early land plants. *Palaeontology*. 15:365-377.
- BOWER, F. O. 1935. *The Origin of a Land Flora*. Macmillan; London.
- CHALONER, W. G. AND A. SHEERIN. 1979. Devonian macrofloras. The Devonian System. Spec. Pap. Palaeontol. 23:145-161.
- FISHER, J. B. AND H. HONDA. 1979. Branch geometry and effective leaf area: a study of *Terminalia*-branching pattern. I. Theoretical trees. *Am. J. Bot.* 66:633-644.
- GATES, D. M. 1965. Energy, plants, and ecology. *Ecology*. 46:1-16.
- GATES, D. M. 1970. Physical and physiological properties of plants. Pp. 224-252. In: *Remote Sensing*. Natl. Acad. Sci.; Washington, D.C.
- GIBBS, J. B. AND D. T. PATTEN. 1970. Plant temperatures and heat flux in a Sonoran Desert ecosystem. *Oecologia (Berl.)*. 5: 165-184.
- GOEBEL, K. 1889. *Pflanzenbiologische Schilderungen*. 1. Teil. Elwert; Marburg, Germany.
- HALLÉ, F. R., A. A. OLDEMAN, AND P. B. TOMLINSON. 1978. *Tropical Trees and Forests: An Architectural Analysis*. Springer-Verlag; Heidelberg.
- HONDA, H. 1971. Description of the form of trees by the parameters of the tree-like body; effects of the branching angle and the branch length on the shape of the tree-like body. *J. Theoret. Biol.* 31:331-338.
- HONDA, H., P. B. TOMLINSON, AND J. B. FISHER. 1981. Computer simulation of branch interaction and regulation of unequal flow rates in botanical trees. *Am. J. Bot.* 68:569-585.
- HORSFIELD, K. 1967. Morphology of the human bronchial tree. M.D. thesis, Univ. Birmingham.
- KONIS, E. 1950. On the temperature of *Opuntia* joints. *Palestine J. Bot.*, Jerusalem ser. 5:46-55.
- MCMAHON, T. A. AND R. E. KRONAUER. 1976. Tree structure: deducing the principle of mechanical design. *J. Theoret. Biol.* 59: 443-466.
- MONSI, M. AND T. SAEKI. 1953. Über den Lichtfaktor in den Pflanzengesellschaften und seine Bedeutung für die Staffproduktion. *Jap. J. Bot.* 14:22-52.
- MURRAY, C. D. 1926a. The physiological principle of minimum work. I. The vascular system and the cost of blood volume. *Proc. Nat. Acad. Sci.* 12:207-214.
- MURRAY, C. D. 1926b. The physiological principle of minimum work. II. Oxygen exchange in capillaries. *Proc. Nat. Acad. Sci.* 12:299-304.
- MURRAY, C. D. 1926c. The physiological principle of minimum work applied to the angle of branching of arteries. *J. Gen. Physiol.* 9:835-841.
- MURRAY, C. D. 1927. A relationship between circumference and weight in trees and its bearing on branching angles. *J. Gen. Physiol.* 10:725-729.
- NIKLAS, K. J. 1976. The role of morphological biochemical reciprocity in early land plant evolution. *Ann. Bot. (Lond.)*. 40:1239-1254.
- NIKLAS, K. J. 1982. Computer simulations of early land plant branching morphologies: canalization of patterns during evolution. *Paleobiology*. 8:196-210.
- NIKLAS, K. J. AND T. D. O'ROURKE. 1982. Growth patterns of plants that maximize vertical growth and minimize internal stresses. *Am. J. Bot.* 69:1367-1374.
- NIKLAS, K. J., B. H. TIFFNEY, AND A. H. KNOLL. 1980. Apparent changes in the diversity of land plants. Pp. 1-89. In: Hecht, M. K., W. C. Steere, and B. Wallace, eds. *Evolutionary Biology*. Vol. 12. Plenum; New York.
- NISBET, R. A. AND D. T. PATTEN. 1974. Seasonal temperature acclimation of a prickly-pear cactus in south-central Arizona. *Oecologia (Berl.)*. 15:345-352.
- NOBEL, P. S. 1980. Interception of photosynthetically active radiation by cacti of different morphology. *Oecologia (Berl.)*. 45: 160-166.
- NOBEL, P. S. 1981. Influences of photosynthetically active radiation on cladode orientation, stem tilting, and height of cacti. *Ecology*. 62:982-990.
- NOBEL, P. S. 1982. Orientation, PAR interception, and nocturnal acidity increases for terminal cladodes of a widely cultivated cactus, *Opuntia ficus-indica*. *Am. J. Bot.* 69:1462-1469.
- RAND, R. H. 1983. Fluid mechanics of green plants. *Ann. Rev. Fluid Mech.* 15:29-45.
- RAND, R. H. AND J. R. COOKE. 1978. Fluid mechanics of phloem flow: an axisymmetric model. *Trans. ASAE*. 21:898-900, 906.
- RAND, R. H., S. K. UPADHYAYA, AND J. R. COOKE. 1980. Fluid dynamics of phloem flow. II. An approximate formula. *Trans. ASAE*. 23:581-584.
- SHINOZAKI, K. K. Y., K. HOZUMI, AND T. KIRA. 1964. A quantitative analysis of plant form: the pipe model theory. I. Basic analysis. *Jap. J. Ecol.* 14:97-105.
- THORNLEY, J. H. M. 1977. A model of apical bifurcation applicable to trees and other organisms. *J. Theoret. Biol.* 64:165-176.
- TOMLINSON, P. B. 1983. Tree architecture. *Am. Sci.* 71:141-149.
- TOMLINSON, P. B. AND A. M. GILL. 1973. Growth habits of tropical trees: some guiding principles. In: Meggers, B. J., E. S. Ayensu, and W. D. Duckworth, eds. *Tropical Forest Ecosystems in Africa and South America*. Smithsonian Inst. Press; Washington, D.C.
- WHITE, J. 1979. The plant as a metapopulation. *Annu. Rev. Syst. Ecol.* 10:109-145.
- WHITNEY, G. G. 1976. The bifurcation ratio as an indicator of adaptive strategy in woody plant species. *Bull. Torrey Bot. Club.* 103:67-72.
- WILSON, B. F. AND R. R. ARCHER. 1977. Reaction wood: induction and mechanical action. *Annu. Rev. Plant Physiol.* 28:23-43.
- WOODHOUSE, R. M., J. G. WILLIAMS, AND P. S. NOBEL. 1980. Leaf orientation, radiation interception, and nocturnal acidity increases by the CAM plant *Agave deserti* (Agavaceae). *Am. J. Bot.* 67:1179-1185.
- ZIMMERMANN, M. H. 1978. Structural requirements for optimal water conduction in tree systems. Pp. 517-532. In: Tomlinson, P. B. and M. H. Zimmermann, eds. *Tropical Trees as Living Systems*. Cambridge Univ. Press; Cambridge.
- ZIMMERMANN, W. 1930. Der Baum in seinem phylogenetischen Werden. *Berlin Bot. Ges.* 48:34-49.